

Review Article

Manganese-enhanced magnetic resonance imaging (MEMRI): methodological and practical considerations

Afonso C. Silva,^{1*} Jung Hee Lee,¹ Ichio Aoki² and Alan P. Koretsky¹

¹Laboratory of Functional and Molecular Imaging, National Institutes of Neurological Disorders and Stroke, Bethesda, MD, USA

²Department of Medical Informatics, Meiji University of Oriental Medicine, Kyoto, Japan

Received 15 October 2004; Revised 20 October 2004; Accepted 20 October 2004

ABSTRACT: Manganese-enhanced MRI (MEMRI) is being increasingly used for MRI in animals due to the unique T_1 contrast that is sensitive to a number of biological processes. Three specific uses of MEMRI have been demonstrated: to visualize activity in the brain and the heart; to trace neuronal specific connections in the brain; and to enhance the brain cytoarchitecture after a systemic dose. Based on an ever-growing number of applications, MEMRI is proving useful as a new molecular imaging method to visualize functional neural circuits and anatomy as well as function in the brain *in vivo*. Paramount to the successful application of MEMRI is the ability to deliver Mn^{2+} to the site of interest at an appropriate dose and in a time-efficient manner. A major drawback to the use of Mn^{2+} as a contrast agent is its cellular toxicity. Therefore, it is critical to use as low a dose as possible. In the present work the different approaches to MEMRI are reviewed from a practical standpoint. Emphasis is given to the experimental methodology of how to achieve significant, yet safe, amounts of Mn^{2+} to the target areas of interest. Copyright © 2004 John Wiley & Sons, Ltd.

KEYWORDS: manganese; animal models; brain; heart; contrast-agents; rat; mouse; imaging

INTRODUCTION

Manganese-enhanced MRI (MEMRI) is being increasingly used for MRI in animals due to the unique T_1 contrast that is sensitive to a number of biological processes. Thus far, three specific uses of MEMRI for imaging the animal brain have been demonstrated. First, due to the fact that manganese ion (Mn^{2+}) can enter excitable cells via voltage gated calcium channels, protocols have been devised that enable accumulation of Mn^{2+} in active areas of the brain^{1–4} and heart.^{5,6} This technique has been referred to as activation-induced MEMRI (AIM-MRI).^{1,3,4} The second use of MEMRI is to trace specific neuronal connections in the brain. MEMRI has been shown to enable imaging anterograde connections in the olfactory,^{7,8} visual,^{9–11} and somatosensory pathways¹² of the rat and mouse brain after direct injection of $MnCl_2$

into a specific brain region. The song centers of the bird¹³ and neural connections in the monkey¹⁴ have also been mapped with MEMRI neuronal tracing techniques. The third use of MEMRI has been as a whole-brain contrast agent after systemic administration.^{2,15–17} It has been demonstrated in mice and rats that an intraperitoneal, intravenous or subcutaneous injection of $MnCl_2$ leads to unique MRI contrast of the brain.^{1,2,15–17} Taken together, MEMRI is proving useful as a new molecular imaging method to visualize functional neural circuits and anatomy in the brain *in vivo*.

Paramount to the successful application of MEMRI for the three major classes of experiments mentioned above is the ability to deliver Mn^{2+} to the site of interest at an appropriate dose and in a time-efficient manner. A major drawback to the use of Mn^{2+} as a contrast agent is its cellular toxicity. It is well known that chronic exposure to manganese leads to a neurological disorder resembling Parkinson's disease,¹⁸ and acute overexposure to Mn^{2+} can also lead to hepatic failure¹⁹ and cardiac toxicity.²⁰ Therefore, it is critical to use as low a dose as possible. Nevertheless, MR relaxation rates are proportional to the effective concentration of Mn^{2+} in tissue, and thus significant amounts of Mn^{2+} are required to produce robust and detectable contrast.

The goal of optimizing MEMRI pulse sequences and strategies for efficient delivery of manganese to the target

*Correspondence to: A. C. Silva, Cerebral Microcirculation Unit, Laboratory of Functional and Molecular Imaging, National Institute of Neurological Disorders and Stroke, National Institutes of Health, 10 Center Drive, Building 10, Room B1D106 Bethesda, MD 20892-1065, USA.

E-mail: SilvaA@ninds.nih.gov

Abbreviations used: APit, anterior lobe of PIT; CEB, cerebellum; DG, dentate gyrus; IP, interpeduncular nucleus; IPit, intermediate lobe of PIT; MEMRI, manganese-enhanced MRI; MSDS, material safety data sheets; OB, olfactory bulb; Pi, pineal gland; Pit, pituitary gland; PPit, posterior lobe of PIT.

organ of interest, while minimizing toxicity to the animal, leaves the investigator with the question of 'How best to perform MEMRI experiments?' In the present work the different approaches to MEMRI are reviewed from a practical standpoint. Emphasis is given to the experimental methodology of how to deliver significant, yet safe, amounts of Mn^{2+} to the target areas of interest.

MANGANESE CHLORIDE AS A SOURCE OF Mn^{2+}

Preparation of $MnCl_2$ solution

The simplest way to deliver Mn^{2+} to the animal is to use a solution of $MnCl_2$. This salt is easily available from any major biochemical company, and may be available in different grades, such as in a purified (> 99%) anhydrous form, $MnCl_2$ (for example, product number 244589 from Sigma-Aldrich Corp., St Louis, MO, USA), which comes in powder form and has a molecular weight of 125.84 g/mol; or as a highly purified (99.999%) hydrated form, $MnCl_2 \cdot 4H_2O$ (for example, product number 529680 from Sigma-Aldrich Corp.), which comes in flake form and which has a molecular weight of 197.9 g/mol. Whichever form of $MnCl_2$ is used, it is important to properly dilute it into a solution with concentration and chemical characteristics compatible with the biological system of interest. There has been little work studying whether different salts of Mn^{2+} significantly alter the detected contrast, and this may be an important aspect for future research.

Physical and chemical properties of the solution to be injected, such as osmolarity and pH, ought to be considered to ensure successful applications. The body fluid has an osmolarity of approximately 300 mOsm/l.²¹ If substantial amounts of $MnCl_2$ are to be infused to the body in a systemic fashion, one should ensure that the infusion will not significantly alter the natural osmolarity of body fluids. This care can be properly observed with the use of an isotonic solution of $MnCl_2$. Because each mole of $MnCl_2$ equals 3 Osm, concentrations around 100 mM are required. Solutions significantly below such concentration will be hypotonic, while solutions significantly above 100 mM will be hypertonic. Whether the tonicity of the $MnCl_2$ solution will play an important effect on the experiment depends on the relative volume of infusion with respect to the target tissue. For systemic infusions, such as intravenous or intraperitoneal administration, the tonicity of the solution may be of little consequence, but for targeted injections, such as stereotaxic brain infusions,^{12–14,22} it may have a strong local impact.

The same argument made above with respect to the tonicity of the $MnCl_2$ solution is valid for its pH. The pH of a 100 mM $MnCl_2$ solution in deionized water, at room temperature, is 5.5–5.8 (unpublished data). A useful buffer to keep the pH within physiological levels for

use with $MnCl_2$ solution is bicine (product number B3876, Sigma-Aldrich Co., St Louis, MO, USA) dissolved to 100 mM in deionized water and adjusted to pH 7.4 using NaOH.²² $MnCl_2$ is then added to the bicine solution at 100 mM concentration. This recipe should provide the investigator with a solution of $MnCl_2$ at physiological pH, which is suitable for most MEMRI experiments.

Toxicity of manganese

A major drawback to the use of Mn^{2+} as an MR detectable contrast agent is its cellular toxicity, and thus a critical issue for eventual extension of MEMRI for use in humans is to use as low a dose as possible. Indeed, toxic effects in animals discouraged the early development of Mn^{2+} as an MRI contrast agent.²⁰

The material safety data sheet (MSDS) for manganese chloride cites this substance as a harmful chemical that causes skin or eye irritation upon contact, and which may be harmful if absorbed through the skin or if ingested. Because the material is irritating to mucous membranes and upper respiratory tract, one should wear proper barriers when manipulating this material, to avoid direct skin contact and to avoid breathing the powder. According to the MSDS for $MnCl_2$, the target organs include the central nervous system and the lungs, and the following signs and symptoms of exposure have been identified: 'Men exposed to manganese dusts showed a decrease in fertility. Chronic manganese poisoning primarily involves the central nervous system. Early symptoms include languor, sleepiness and weakness in the legs. A stolid mask-like appearance of the face, emotional disturbances such as uncontrollable laughter and a spastic gait with tendency to fall in walking are findings in more advanced cases. High incidence of pneumonia has been found in workers exposed to the dust or fume of some manganese compounds.' Manganese is also known to be a potential mutagen.²³

Table 1 shows the LD₅₀ acute toxicity data listed in the MSDS for $MnCl_2$. Doses as low as 93 mg/kg for rats or 38 mg/kg for mice show significant adverse effects and mortality rates. However, current MEMRI experiments are being performed at similar doses, or higher, as shown in Table 2, with good results and few adverse effects reported. For example, we have been able to reliably administer up to 175 mg/kg intravenously in rats up to 250 g body weight,¹⁵ and in mice up to 25 g body weight²⁴ with only minor and temporary side effects that resolved slowly over 30–60 min after administration. Particular experimental details and procedures, such as the concentration of the $MnCl_2$ solution, the rate of infusion and the route of administration, temperature of the solution and anesthetic levels seem to play an important role in determining the maximum effective dose that can be safely administered without major side effects.

Table 1. Toxicity data (LD₅₀) for MnCl₂

Species	Route	Dose	Remarks
Rat	Oral	250 mg/kg	
	Intraperitoneal	147 mg/kg	Behavioral: somnolence (general depressed activity) Behavioral: convulsions or effect on seizure threshold
	Intravenous	92.6 mg/kg	Behavioral: somnolence (general depressed activity) Behavioral: convulsions or effect on seizure threshold
Mouse	Intramuscular	700 mg/kg	
	Oral	1031 mg/kg	Behavioral: tremor Behavioral: convulsions or effect on seizure threshold Lungs, thorax or respiration: other changes
	Intraperitoneal	121 mg/kg	
	Intravenous	38 mg/kg	Behavioral: somnolence (general depressed activity) Behavioral: ataxia Lungs, thorax or respiration: respiratory stimulation
	Intramuscular	255 mg/kg	
Dog	Intravenous	202 mg/kg	
Guinea pig	Oral	916 mg/kg	Behavioral: tremor Behavioral: convulsions or effect on seizure threshold Lungs, thorax or respiration: other changes

Source: MSDS for MnCl₂ (product number 244589, Sigma-Adrich, St Louis, MO, USA).

Table 2. Systemic doses of MnCl₂ used in current MEMRI experiments

Species	Route	Dose	Reference
Rat	Intravenous	54 mg/kg	Lin and Koretsky ¹
	Intravenous	60 mg/kg	Duong <i>et al.</i> ³
	Intra-arterial	53 mg/kg	Aoki <i>et al.</i> ⁴
Mouse	Intravenous	175 mg/kg	Aoki <i>et al.</i> ¹⁵
	Nasal	65 mg/kg	Pautler <i>et al.</i> ⁷
	Intravenous	175 mg/kg	Lee <i>et al.</i> ²⁴
	Intravenous	6.6 mg/kg	Hu <i>et al.</i> ⁵
	Intraperitoneal	20 mg/kg	Watanabe <i>et al.</i> ¹⁷

OPTIMIZATION OF MRI PARAMETERS FOR MEMRI

Manganese ion is known to shorten both the T_1 as well as the T_2 relaxation times of surrounding water, making it an excellent MR detectable contrast agent.^{25,26} There is a proportional relationship between the water R_1 ($= 1/T_1$) and R_2 ($= 1/T_2$) relaxation rates and the concentration of Mn^{2+} :

$$R_{1,2}([Mn^{2+}]) = R_{1,2}(0) + \chi_{1,2} \cdot [Mn^{2+}] \quad (1)$$

where $[Mn^{2+}]$ indicates the concentration of Mn^{2+} (mM), $R_{1,2}([Mn^{2+}])$ indicates the mean water R_1 or R_2 relaxation rates (1/s) at a given $[Mn^{2+}]$, and $\chi_{1,2}$ is the T_1 or T_2 relaxivity ($s^{-1} mM^{-1}$) of manganese.

Extensive measurements of χ_1 and χ_2 have been performed *in vitro* as well as in tissue.^{27–31} *In vitro* values for χ_1 are on the order $7–8 s^{-1} mM^{-1}$ for fields above 1.5 T,^{27,28,30} while χ_2 values are in the range $30–125 s^{-1} mM^{-1}$,^{27,28,30} increasing with magnetic field strength. *In vivo*, relaxivity constants can be up to one

order of magnitude higher,^{27,29} due to binding of Mn^{2+} to macromolecules. Equation (1) indicates that the effects of Mn^{2+} on tissue water can be observed with T_1 - or T_2 -weighted sequences consisting of either saturation–recovery or inversion–recovery sequences performed at optimized repetition times (TR) and echo times (TE). Therefore, optimization of the MRI parameters is necessary in order to achieve maximum contrast between tissues that uptake different amounts of $MnCl_2$. The MR signal of a spin population imaged in a saturation–recovery spin-echo sequence can be described as:

$$\hat{\rho}(TR, TE) = \rho_0 \cdot (1 - e^{-TR \cdot R_1}) \cdot e^{-TE \cdot R_2} \quad (2)$$

where all parameters have the standard definitions (for gradient-echo sequence, R_2 is replaced with R_2^*). The contrast between two spin populations of similar densities ρ_0 , one of which contains a uniform concentration of Mn^{2+} , is given by:

$$C([Mn^{2+}], TR, TE) = \rho_0 \cdot \left(1 - e^{-TR \cdot R_1([Mn^{2+}])}\right) \times e^{-TE \cdot R_2([Mn^{2+}])} - \rho_0 \cdot \left(1 - e^{-TR \cdot R_1(0)}\right) \cdot e^{-TE \cdot R_2(0)} \quad (3)$$

Substituting eqn (1) into eqn (3) will provide the following expression for the contrast as a function of the concentration of Mn^{2+} , TR and TE :

$$C([Mn^{2+}], TR, TE) = \rho_0 \times \left[\left(1 - e^{-TR \cdot \chi_1 \cdot [Mn^{2+}]} \cdot e^{-TE \cdot \chi_2 \cdot [Mn^{2+}]}\right) \times e^{-TR \cdot R_1(0)} - \left(1 - e^{-TE \cdot \chi_2 \cdot [Mn^{2+}]}\right) \right] \cdot e^{-TE \cdot R_2(0)} \quad (4)$$

Equation (4) shows that R_1 and R_2 have opposing and competing effects on contrast. As the concentration of manganese increases, for any given set of TR and TE

parameters, the contrast increases due to R_1 effects, and decreases due to R_2 effects. Therefore, it is necessary for the investigator to choose whether a T_1 -based contrast or a T_2 -based contrast is desired.

Figure 1 shows plots of the contrast as a function of TR [Fig. 1(A)] and of TE [Fig. 1(B)] for different $[\text{Mn}^{2+}]$. In both cases, fully relaxed conditions were used, i.e. Fig. 1(A) plots eqn (4) as a function of TR for $TE = 0$, and Fig. 1(B) shows eqn (4) as a function of TE for $TR = \infty$. Owing to the much larger tissue T_1 than T_2 , T_1 -based contrast is more sensitive to lower amounts of Mn^{2+} . In addition, T_1 -based contrast is the option of choice, because positive enhancement is created, with higher signal-to-noise, in addition to higher contrast-to-noise. If T_2 contrast were to be used, the signal would decrease with increasing $[\text{Mn}^{2+}]$ [Fig. 1(B)], and potential spatial distortions or blurring of the image could occur because of the shorter transverse relaxation time of water. Therefore, T_1 -weighting is usually the chosen route, and experiments should be performed using the shortest TE allowed by the spectrometer to minimize both T_2 and T_2^* degrading effects on the image. Note that the minimum TE will be constrained by acquisition parameters, such as acquisition bandwidth, matrix size and

gradient strength, and may not be short enough compared with T_2 and T_2^* , especially at high magnetic field strengths. However, if it is possible to choose TE such that $TE \ll T_2, T_2^*([\text{Mn}^{2+}])$, then eqn (4) simplifies to:

$$C([\text{Mn}^{2+}], TR, TE \rightarrow 0) = \rho_0 \cdot \left(1 - e^{-TR \cdot \chi_1 \cdot [\text{Mn}^{2+}]}\right) \cdot e^{-TR \cdot R_1(0)} \quad (5)$$

and both gradient-echo as well as spin-echo sequences should yield similar contrast. Differentiating with respect to TR will yield the following expression for the optimal TR that maximizes eqn (5):

$$TR_{\text{opt}}([\text{Mn}^{2+}]) = \frac{\ln(R_1[\text{Mn}^{2+}]) - \ln[R_1(0)]}{[R_1[\text{Mn}^{2+}] - R_1(0)]} \quad (6)$$

Figure 1(A) shows a plot of the contrast as a function of TR for different $[\text{Mn}^{2+}]$. It is clear that the higher the $[\text{Mn}^{2+}]$, the shorter the optimal TR . It should be noted that, because of the dependence of TR_{opt} on $[\text{Mn}^{2+}]$, it may be difficult to choose a TR that maximizes overall contrast if different amounts of Mn^{2+} are uptaken by different sub-organs or regions of the brain. Furthermore, eqn (6) does not factor in the total acquisition time. For high-resolution animal studies that employ large three-dimensional matrices, acquisition time can become a considerable burden, and most likely the investigator will favor a shorter, sub-optimal repetition time that constrains the experiment to a reasonable time, rather than use the optimal TR that will require an impractically long scan. The optimization provided by eqn (6) is best suited for tract-tracing experiments or for localized injections of Mn^{2+} , when a more uniform $[\text{Mn}^{2+}]$ is expected over a better defined region than the distribution obtained by employing systemic administration.

SYSTEMIC ADMINISTRATION OF MnCl_2

The earliest work with Mn^{2+} as an MRI contrast agent relied on giving a systemic dose of Mn^{2+} —usually as the chloride salt—and monitoring distribution in a number of tissues.^{32,33} Indeed, Mn^{2+} accumulates in almost all tissues when administered systemically, either intravenously, intraperitoneally or intramuscularly. Significant accumulation was detected early in many tissues such as liver, kidney, heart and brain.^{20,27,32,33} More recently, with significant and progressive improvements in MRI technology, which translate into increases in sensitivity and spatial resolution, there is renewed interest in the many applications of Mn^{2+} as a biological MRI detectable contrast agent.

Manganese is an intracellular contrast agent

There were two key results derived from studies of tissue enhancement caused by Mn^{2+} . The first one is that MRI

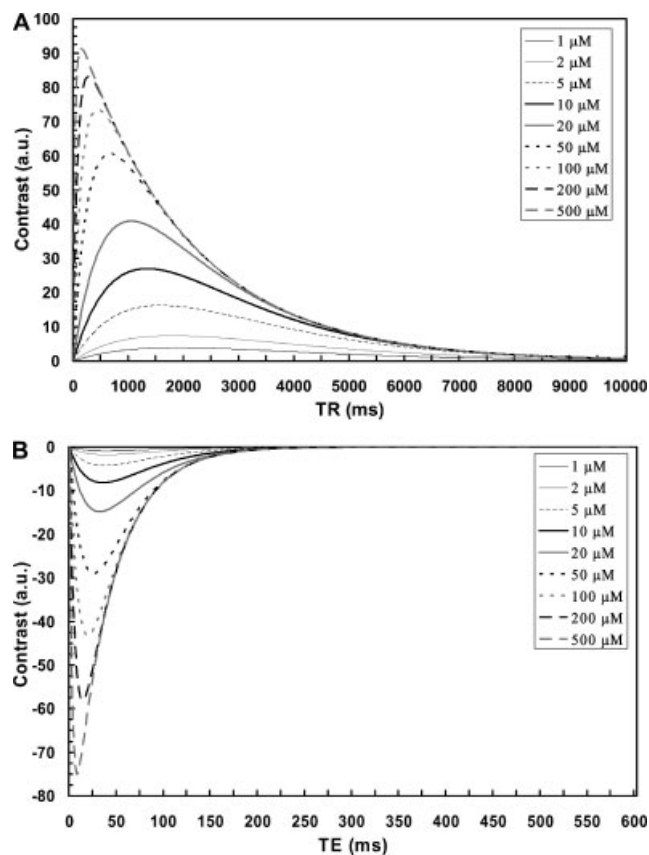


Figure 1. Signal contrast as a function of TR (A) and TE (B) for different tissue concentrations of manganese. The optimal TR that maximizes contrast between tissue that has manganese versus tissue that does not uptake manganese decreases as the manganese concentration increases

contrast after systemic MnCl_2 comes from intracellular Mn^{2+} .^{20,27,32–34} This is based on the fact that tissue enhancement lasts long after blood enhancement and that the volume distribution agrees with the intracellular volume. Unlike chelated gadolinium contrast agents, which remain extracellular, Mn^{2+} offers a unique viewpoint of tissue, mapping signal intensities according to its cellular density. This property has been very useful for visualization of the brain cytoarchitecture, and is discussed in further detail below.

The second central conclusion is that the rate of uptake of Mn^{2+} serves as a reliable marker of normal tissue function. Normal uptake into a tissue entails normal function. Pathological conditions associated, for example, with tumor or ischemia, are amenable to detection due to differential uptake of Mn^{2+} . Once again in this case the use of Mn^{2+} as an MRI contrast agent has been inhibited due to toxicity in the animal models tested.²⁰ Nevertheless, chelates of Mn^{2+} were developed to assess tissue function. Manganese dipyrroldiphosphate (MnDPDP), an FDA approved contrast agent used for imaging of the liver, has been used for negative enhancement of hepatic abnormalities.³⁵ Furthermore, MnDPDP has been successfully utilized for imaging cardiac ischemia.^{34,36–38} It is interesting to note that much of the Mn^{2+} in MnDPDP comes off the chelate slowly after administration,³⁹ which implies some of the tissue enhancement detected with MnDPDP was due to Mn^{2+} .

Systemic administration of manganese enhances the brain cytoarchitecture

The neurotoxicity of Mn^{2+} , manifested mainly by the incidence of movement disorders in people chronically overexposed,⁴⁰ has led the use of MRI to search for areas that accumulate high levels of Mn^{2+} . The accumulation of Mn^{2+} in basal ganglia and other areas of the brain following systemic administration has been demonstrated in rat,^{41,42} monkeys,⁴³ and humans.⁴⁴ In basal ganglia, chronic accumulation of high levels of Mn^{2+} may lead to cell death and cause symptoms similar to Parkinson's disease. Out of those studies, aimed at elucidating the pathophysiology associated with manganese, came the notion that systemic administration of Mn^{2+} is a simple way to enhance the cytoarchitecture of the brain in MRI. Indeed, recent work in rat and mouse shows that doses of MnCl_2 that do not have toxic effects lead to useful contrast for MRI of the brain.^{2,15–17}

Figure 2 shows typical coronal, horizontal and sagittal views from three-dimensional T_1 -weighted data sets of a rat [Fig. 2(A)] and of a wild-type mouse [Fig. 2(B)], 24 h following a systemic intravenous injection of 175 mg/kg MnCl_2 . The manganese-enhanced structures are well visualized in all three-dimensional orientations. Both in mouse as well as in rat, the contrast enhancement of the brain anatomy is superb, showing excellent cytoarchitectonic details of the neuroarchitecture due to the presence of Mn^{2+} in regions such as the hippocampus, pituitary

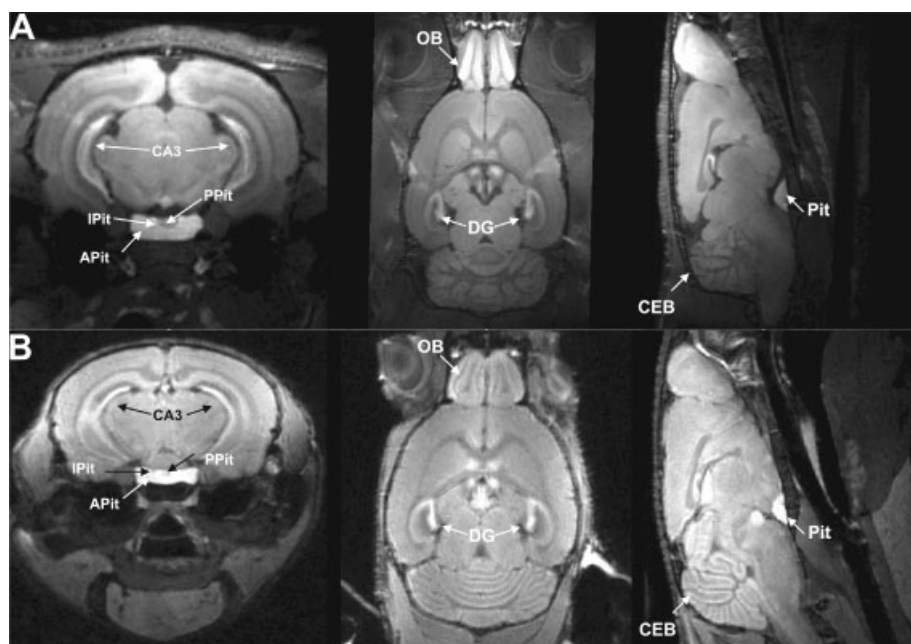


Figure 2. High-resolution ($100 \times 100 \times 100 \mu\text{m}^3$), T_1 -weighted three-dimensional MRI of the rodent brain 24 h following systemic application of MnCl_2 . (A) Coronal (left), horizontal (middle) and sagittal (right) views of a rat brain, showing excellent cytoarchitectonic contrast due to the presence of Mn^{2+} in regions such as the hippocampus (CA3 and DG), pituitary gland (Pit) and its major lobes (APit, IPit, PPit), cerebellum (CEB) and olfactory bulb (OB). (B) Corresponding views of a mouse brain

gland (Pit), cerebellum (CEB) and olfactory bulb (OB). In the coronal view, the hippocampus is enhanced with clear delineation of the CA3 and the dentate gyrus (DG) regions. The Pit is well depicted both on the coronal as well as on the sagittal views, and Mn^{2+} allows clear separation of the posterior (PPit), intermediate (IPit) and anterior (APit) lobes. The horizontal sections show enhancement of periventricular zones, the CA1, CA2, CA3 and the fimbria (fi) regions of hippocampus, the arrow-head of DG, and layers of OB. In the sagittal view, CEB shows excellent gray–white matter contrast, together with Pit and DG.

Dose-dependent brain contrast

Recent work has shown that MRI after systemic administration of $MnCl_2$ leads to unique contrast that highlights a number of features of cytoarchitecture in the rodent brain.^{2,15–17} In these studies, either a subcutaneous injection of a low dose (20 mg/kg)¹⁷ or intraperitoneal, intravenous or subcutaneous injection of high doses (175 mg/kg) were used.^{2,15} We have recently performed a study to address the contrast in the brain as a function of administered dose of $MnCl_2$.²⁴ We showed that a wide range of systemic doses (9–175 mg/kg) leads to MRI detection of the same features described previously. Figure 3(A) shows sagittal MEMRI of the mouse brain acquired at 11.7 T at varying doses of infused $MnCl_2$. Enhancement of the brain is clearly visible even at the lowest dose of $MnCl_2$, especially in the areas of the brain which lack a BBB, such as Pit and the pineal gland (Pi). In addition, enhancements in the periventricular regions (pv) and in OB were clearly detected even at the lowest doses used. With as little as one-tenth of the maximum dose, areas such as the hippocampus, the interpeduncular nucleus (IP) and the substructures of CEB were strongly enhanced. Such enhancement progressed with increasing doses of $MnCl_2$, and in general both the contrast as well as the signal–noise ratio (SNR) of the enhanced regions was increased, allowing for better delineation of sub-regional anatomical features, particularly within hippocampus, cortex and deep brain nuclei. Consistent with earlier studies, OB layers, the CA formation of the hippocampus, gray matter in CEB, as well as numerous other regions of the brain were enhanced by Mn^{2+} . Also consistent with earlier studies was the detection of other features of neuroarchitecture at the highest doses of infused $MnCl_2$ such as the cortical layers.^{2,15} Indeed, detection of cortical layers in mouse brain became significant only above 88 mg/kg, and improved with doses up to 175 mg/kg, the maximum dose tested in our study.²⁴ Such results clearly indicate that there is dose dependence to some of the features of the neuroarchitecture detectable by systemic MEMRI, but also suggest that the amount of Mn^{2+} reaching the brain after a systemic injection is still relatively small, and that further

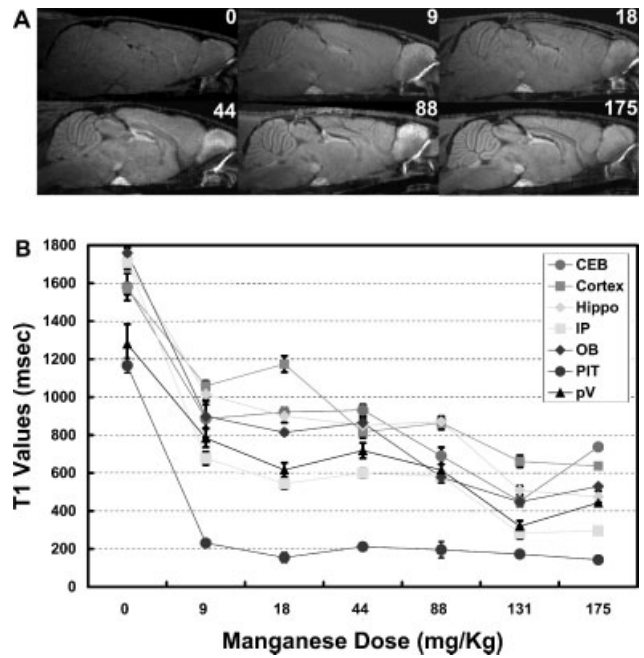


Figure 3. (A) Contrast dependence on systemic dose of $MnCl_2$. Typical sagittal cuts from representative 3D-MEMRI are shown at varying doses of $MnCl_2$, indicated at each panel in units of mg $MnCl_2$ /kg body weight. Enhancement of the brain is clearly visible even at the lowest dose of $MnCl_2$ (9 mg/kg, top row, middle), especially in the areas of the brain devoid of the BBB, such as the pituitary and the pineal glands, in periventricular zones, and in olfactory bulb. Tissue-specific enhancement progressed with increasing doses of $MnCl_2$, and in general both the contrast as well as the SNR of the enhanced regions, allowing for better delineation of sub-regional anatomical features, particularly within hippocampus, olfactory bulb, cortex, and deep brain nuclei. See Fig. 2 for labeling of different anatomical structures. (B) Dependence of T_1 values on systemic dose of $MnCl_2$ across various regions of the mouse brain. T_1 values were obtained in the pituitary gland (Pit), periventricular tissue (pv), hippocampus (HP), cortex, interpeduncular nucleus (IP), cerebellum (CEB) and olfactory bulb (OB). A significant decrease in T_1 values was noticeable in all regions at all doses of $MnCl_2$. Regions devoid of the BBB, such as the pituitary gland, showed a dose-independent saturation in post- $MnCl_2$. For all other regions, T_1 continued to decrease with increasing doses of $MnCl_2$. [Adapted and reproduced from Lee JH, Silva AC, Merkle H, Koretsky AP. Manganese-enhanced MRI (MEMRI) of mouse brain after systemic administration of $MnCl_2$: dose dependent and temporal evolution of T_1 contrast. *Magn. Reson. Med.* 2004 (In press), Copyright © 2004 John Wiley & Sons, Inc. Reprinted with permission of Wiley-Liss, Inc., a subsidiary of John Wiley & Sons, Inc.]²⁴

refinement of MEMRI is needed in order to permit reliable detection of the fine details of the brain cytoarchitecture.

In order to quantify the dose dependence of the MRI enhancement, T_1 maps were obtained at different doses of $MnCl_2$, and T_1 values across different brain regions were quantified.²⁴ As shown in Fig. 3(B), a significant decrease in T_1 values was noticeable in all regions at the lowest doses of $MnCl_2$. T_1 continued to decrease with increasing

doses in all regions. However, the changes in T_1 were heterogeneous across different regions of the brain. Regions devoid of the blood–brain barrier (BBB), such as the Pit, showed a larger decrease at the lowest dose and then a much slower decrease with increasing doses of MnCl_2 . This may indicate that Mn^{2+} uptake in the Pit was limited by the ability of the pituitary to transport Mn^{2+} and not by the availability of Mn^{2+} in the blood supply or in the extravascular space surrounding the pituitary. In general the largest changes in T_1 occurred by 44–88 mg/kg, with T_1 getting as short as 200 ms. This large shortening of T_1 explains the large degree of contrast obtained when the brain is imaged at a single TR .

Brain enhancement is temporally heterogeneous

The time-course of distribution of contrast in the period from 0 to 24 h after i.v. administration varies across different regions of the brain.^{15,24} It has been demonstrated that most of the Mn^{2+} enters the brain through the choroid plexus into CSF spaces during the initial 2 h.¹⁵ Figure 4(A) shows the distribution of MnCl_2 in rat brain following systemic i.v. MnCl_2 administration over a 2-week time period.¹⁵ MRI was performed on separate animals before, 2 h, 1 day, 4 days and 14 days after the administration of MnCl_2 . Controls did not receive MnCl_2 and showed very little contrast and low signal in these T_1 -weighted images. Within 2 h of infusion of MnCl_2 , there was large enhancement in the regions with large ventricular space and circumventricular organs such as Pit, Pi and median eminence (Me) in the brain. By 1 day, the enhancement had spread through the brain in a heterogeneous, yet typical distribution. Also by 1 day, the large enhancements in the ventricles detected after 2 h were reduced to pre- MnCl_2 infusion levels. After 1 day, there were no significant changes in the distribution of enhancement, which was still clearly visible at 4 days but declined steadily to near control levels by 14 days.

Figure 4(B) shows the early entry of Mn^{2+} in the brain. Within 5 min after starting the MnCl_2 infusion, the choroid-plexus (CP), Pit and Pi were the first brain structures to enhance [Fig. 4(B), left]. By 10 min, the enhancement diffused to fill up the entire CSF space in the ventricle, including the subarachnoid space [Fig. 4(B), center]. After stopping the infusion and 100 min after first infusing MnCl_2 , the CP lost enhancement and was detected as a darker line within the ventricle, which remained enhanced [Fig 4(B), right]. The initial enhancement of CP, enhancement of CSF and then enhancement of the periventricular tissue was observed in the third and fourth ventricles as well.¹⁵ These findings suggest that Mn^{2+} can cross the blood–CSF barrier via CP, and are in close agreement with the observation that there is a fast transport system for Mn^{2+} into brain through the CP that is 100 times faster than other brain areas.^{45,46}

In addition to the CSF compartment, organs devoid of the BBB, especially Pit and Pi, showed a rapid increase in signal intensity. The wave of high contrast slowly moved out of the ventricular space to redistribute into brain areas in the time period of 2–24 h following administration of MnCl_2 .^{15,24} All around the brain, regions in close proximity to the CSF space, such as pv, fi, hypothalamus, the ventral ends of CA and CEB, the dorsal and intermediate parts of the lateral septal nucleus, the surface of cortex, and the outer surface of OB, showed a gradual enhancement which started 30–60 min after initiating the infusion of Mn^{2+} . These results suggest that manganese is uptaken from CSF to brain tissues via ependyma surrounding ventricles. In particular, enhancement of fi near the lateral ventricle suggested that Mn^{2+} uptake occurs via the choroid fissure and fi to DG and CA.²⁴

Contrast enhancement seems to reach its final pattern 24 h following administration of MnCl_2 . This suggests that there may be a common mechanism for movement of Mn^{2+} from ependyma throughout the brain, which is similar to the anterograde transport of Mn^{2+} along appropriate neuronal pathways.^{47,48} Once it reaches its final pattern, the relative distribution of contrast does not change significantly. However, there is a gradual and slow loss of enhancement over 2–3 weeks.^{24,49} This agrees with previous data that intracranial manganese has an extremely slow clearance rate that can take up to 300 days.^{2,43}

ACTIVITY-INDUCED MANGANESE-ENHANCED MRI (AIM-MRI)

As discussed above, manganese-induced contrast is predominantly intracellular. One of major means of entry of Mn^{2+} into cells is through voltage-gated calcium transporters,^{50–52} which are largely present in excitable cells, such as neurons or myocytes, and open to allow calcium influx during depolarization of the cells. Therefore, Mn^{2+} accumulates in cells through voltage-gated calcium channels in an activity-dependent manner. This concept has been verified by monitoring the quenching of fluorescent calcium indicators caused by the rate of entry of Mn^{2+} into heart cells.⁵³ The rate of fluorescence quenching has been used as a surrogate marker to quantify calcium influx in a variety of cells.⁵⁴ The same notion was used to monitor activity in the brain of rodents with MRI.¹ MnCl_2 was infused intravenously while the brain was stimulated pharmacologically or with somatosensory stimulation.¹ Local increased brain activity led to augmented Mn^{2+} influx and thus to increased contrast on T_1 -weighted MRI. This technique, named activity-induced manganese-enhanced MRI (AIM-MRI), produced strong signal enhancement in appropriate regions of the brain due to activation by glutamate, amphetamines, somatosensory stimulation, and due to awakening from anesthesia as well.^{1,2}

In order to get sufficient accumulation of Mn^{2+} in the active regions of the brain, it is necessary to open the

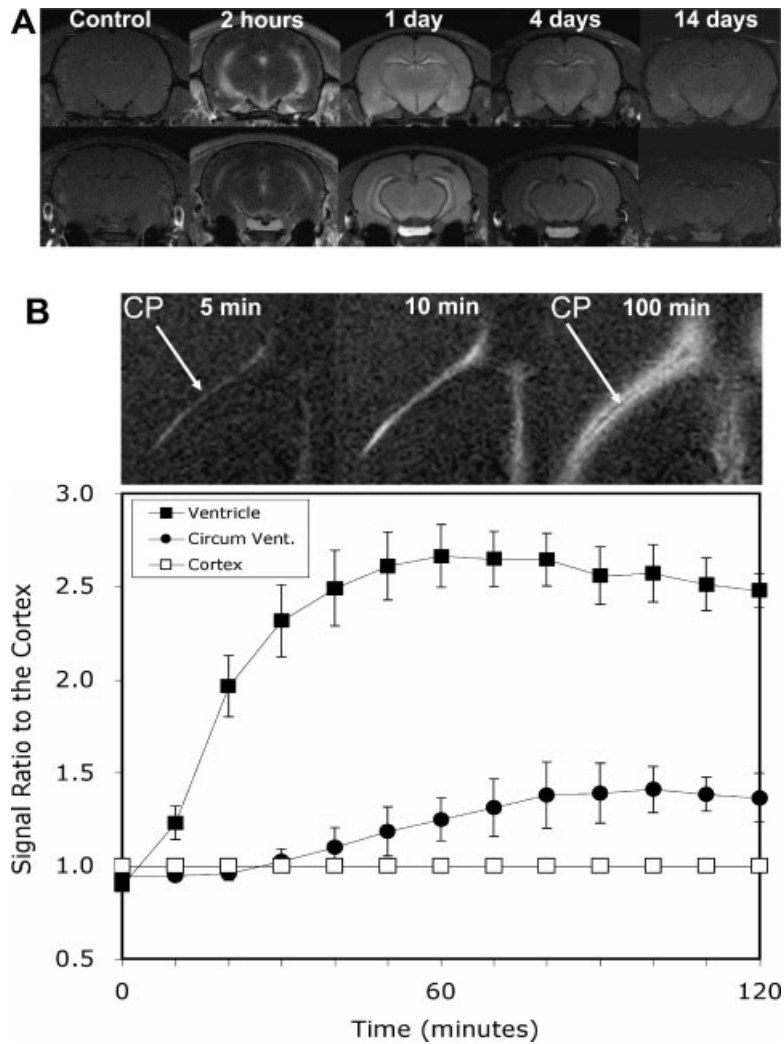


Figure 4. (A) T_1 -weighted MEMRI following the manganese distribution in a rat brain over a 2-week period. MRI was performed on separate animals before (control), 2 h, 1 day, 4 days and 14 days after the administration of $MnCl_2$. Controls did not receive $MnCl_2$ and showed very little contrast and low signal. Within 2 h of infusion of $MnCl_2$, there was large enhancement in the regions with large ventricular space and circumventricular organs such as pituitary, pineal gland and median eminence. By 1 day, the enhancement had spread throughout the brain but showed a heterogeneous, yet typical enhancement. The large enhancements in the ventricles detected after 2 h were reduced to pre- $MnCl_2$ infusion levels. After 1 day, there were no large changes in the distribution of enhancement. Enhancement was clearly visible at 4 days but declined steadily to near-control levels by 14 days. (B) Dynamic imaging of manganese uptake via the choroid plexus, shown via an expanded horizontal view of the left ventricle taken at 5, 10 and 100 min after $MnCl_2$ infusion. Enhancement first occurred highly localized in the lateral ventricle corresponding to the distribution of choroid plexus (CP) (left). By 10 min, the enhancement diffused to fill up the entire CSF space in the ventricle (middle). After stopping the infusion and 100 min after starting infusing $MnCl_2$, the left ventricle remained enhanced, the CP lost enhancement and was detected as a darker line within the ventricle (right). At 100 min after starting to infuse $MnCl_2$, the enhanced region spread into the periventricular brain tissue that touches CSF beyond the region of the left ventricle, such as the fimbria of the hippocampus, and lateral septal nucleus. This is also shown in quantitative MEMRI time-courses of signal normalized to the cortex. [Adapted and reprinted from *Neuroimage*, **22**, Aoki I, Wu YJ, Silva AC, Lynch RM, Koretsky AP. *In vivo* detection of neuroarchitecture in the rodent brain using manganese-enhanced MRI; 1046–1059. Copyright © 2004, with permission from Elsevier.]¹⁵

BBB. This is usually done with a highly concentrated (~25%) solution of D-mannitol, a hypertonic agent that causes temporary and reversible disruption of the BBB.⁵⁵ A few protocols exist that inject mannitol intravenously through the femoral or the tail vein,⁵⁶ or intra-arterially through the common^{1,2} or the external carotid artery.^{3,4} After BBB disruption and upon brain stimulation, Mn^{2+} accumulates in active regions on a short time scale (minutes), but as in the case of systemic administration discussed above, once accumulated it does not leave the regions for several hours. The difference in Mn^{2+} influx and efflux rates offers both an advantage and a disadvantage. The advantage is that Mn^{2+} can be delivered on the bench, outside the MRI, while the animal is being stimulated, and the pattern of activation will be retained for a long time, enabling MRI to be performed well after the stimulus presentation. This opens up interesting experiments in which Mn^{2+} is given to animals while they are behaving in a complex environment. A first step towards this approach was demonstrated when Mn^{2+} was given to an awake, behaving animal, which was later anesthetized and imaged with a T_1 -weighted MRI sequence to probe for specific activity patterns associated with the awake behavior.¹ The disadvantage, however, is that rapid changes in activity, and in particular, deactivation, cannot readily be followed with AIM-MRI.

A comparison between AIM-MRI and hemodynamic-based functional MRI techniques has been performed in rat somatosensory cortex.³ Results showed good overall spatial agreement between the regions mapped by AIM-MRI and the ones mapped by fMRI. However, AIM-MRI presented larger T_1 changes in cortical layer 4, as opposed to BOLD-based fMRI, which detected higher activations near the pial surface where large draining veins are located. This result suggests a better spatial sensitivity for neural activity because AIM-MRI is sensitive to calcium influx. A significant problem for AIM-MRI is the fact that brain electrical activity is strongly dependent on the anesthetic level. Deep anesthesia significantly suppresses activity, making it difficult to detect signal changes. Light anesthesia, on the other hand, may induce stimulus-unrelated, or spatially unspecific, activation. In order to control for the anesthetic depth, a dynamic AIM-MRI technique has been recently proposed that helps reduce non-specific signals associated with AIM-MRI.⁴ In this sequence a baseline activity signal is acquired during infusion of Mn^{2+} , but before presentation of the stimulus, to probe for quiescent rates of Mn^{2+} enhancement unrelated to the intended stimulus paradigm.⁴

AIM-MRI has been utilized in different applications. In a recent work, activation of the hypothalamus induced by osmotic challenges has been studied.⁵⁷ The localization of hypothalamic activation detected by AIM-MRI showed good correspondence with *cfos* expression. Another interesting use of AIM-MRI relates to brain pathophysiology. Because AIM-MRI is sensitive to calcium influx, it should be sensitive to episodes of anoxic

depolarization associated with stroke and cortical spreading depression. An exciting recent result utilized Mn^{2+} infusion to image the excitotoxic phase of stroke, in which a large calcium influx occurs due to a large release of glutamate.⁵⁸

AIM-MRI has been applied to the heart as well. In one study, the rate of Mn^{2+} accumulation in the mouse heart was shown to increase with positive inotropic agents that stimulate calcium influx, and to decrease with calcium channel blockers.⁵ Similarly, in the perfused heart, inhibition of Mn^{2+} influx by calcium channel blockers has been demonstrated.^{28,52,59} The ability of AIM-MRI to be sensitive to cardiac inotropy opens possibilities both for distinguishing viable from non-viable myocardium, as well as for assessing the calcium sensitivity of contraction. Many other tissues should be amenable to AIM-MRI, in particular where electrical activity or ligand-gated calcium channels cause an influx of calcium into cells.

NEURONAL TRACT-TRACING WITH MEMRI

The fact that Mn^{2+} moves along appropriate neuronal pathways is a very useful property for MEMRI applications. Studies designed to determine how environmental Mn^{2+} enters the food supply, and to establish the mechanism for Mn^{2+} distribution in the brain have utilized radioactive isotopes of Mn^{2+} to follow the olfactory pathway in fish and after injection into the rat brain.^{47,60} The combination of the excellent MRI contrast properties of Mn^{2+} and the fact that it moves in neurons was first used to perform MEMRI neuronal tracing in the mouse olfactory and visual pathway.⁷ Pautler *et al.* injected concentrated (2.4 M) $MnCl_2$ solutions into the nose and eye of mice and performed MRI for up to 48 h after injection.^{7,8} MRI enhancement moved from the turbinates to the olfactory bulb and out of the bulb to the primary olfactory cortex, indicating that Mn^{2+} crosses synapses in addition to being transported along neurons. In the eye, MRI enhancement moved down the optic nerve and then into the brain, where enhancement of the superior colliculus could be detected.⁷ Similar results have been obtained in the rat.⁹ In the visual system there was no evidence of trans-synaptic transport. This raises the question of whether the tracing properties of Mn^{2+} vary amongst different neural systems. The use of MRI to measure the transport of Mn^{2+} down the optic nerve has been shown to be a sensitive indicator of damage to the nerve due to radiation.¹¹ This is a clear indication that MEMRI tract-tracing will be useful to study damage and repair of neural connections.

Recently, the use of direct injections of small volumes (10–1000 nl) of $MnCl_2$ (5 mM to 0.8 M) into the brain of birds,¹³ monkeys,¹⁴ and mice⁶¹ to trace neuronal connections has been demonstrated. Injection into one of the song centers in starlings led to delineation of the other

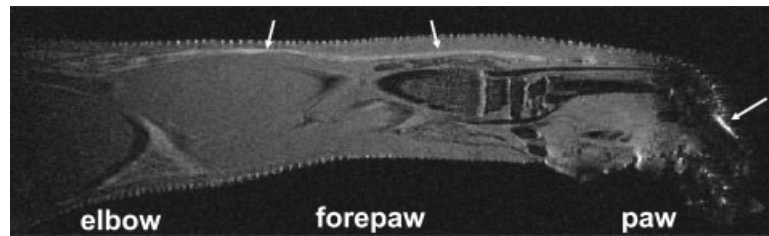


Figure 5. MEMRI tract-tracing of a peripheral nerve in the rat forepaw. $MnCl_2$ mixed in polyethylene glycol was carefully injected to the rat forepaw pad. MRI was obtained 24 hours later, revealing a major peripheral nerve (arrows) running along the entire length of the paw towards the elbow

centers connected to the injected site,¹³ enabling anatomical visualization that could not otherwise be detected by regular MRI. Exciting preliminary data showing changes in size and connectivity of these centers during exposure to specific songs or testosterone^{62,63} indicate that MEMRI will be a useful technique to study brain plasticity. In the monkey it was possible to follow the Mn^{2+} through multiple synapses, demonstrating tracing of extensive neural networks. There was also good agreement with another neuronal tracer, horseradish peroxidase.¹⁴ Similar results were obtained from work in mice, in which injection of Mn^{2+} into the amygdala and striatum showed movement across multiple synapses.⁶¹

An exciting application for non-invasive tracing with MEMRI is to be able to trace peripheral nerves. Figure 5 shows enhancement of a peripheral nerve of the rat forepaw after localized injection of $MnCl_2$ solution mixed in polyethylene glycol to the rat forepaw pad. The forepaw was imaged 1–4 days later. The peripheral nerve showed enhanced signal compared with controls that received only saline, indicating MEMRI is also useful for tracing peripheral nerves. It should also be possible to do direct injections into the peripheral nerves themselves.

CONCLUSIONS

There is rapidly increasing interest in developing MEMRI as a technique for functional and molecular imaging of specific biological processes. It has become clear that the rich biology of Mn^{2+} combined with its potent MRI relaxation properties is leading to exciting new opportunities to probe biological processes in animal models.

Presently, there are three ways to productively use MEMRI. First, simple systemic administration of Mn^{2+} leads to interesting and useful anatomical MRI contrast. The accumulation of Mn^{2+} is enabling analysis of anatomical structures by MRI that would otherwise be difficult to detect. The biological basis for the movement of Mn^{2+} into tissues and its final distribution needs to be more fully determined and this may lead to opportunities for new imaging strategies. Second, a well established way for Mn^{2+} to enter cells is on voltage-gated calcium channels. This has enabled work with MEMRI to probe

activity in brain and heart and the general strategy should be useful for a number of other tissues. Further work needs to be performed to clarify exactly which channels Mn^{2+} can move through to enable AIM-MRI to become a quantitative surrogate of calcium influx. There are no widely used noninvasive imaging techniques that monitor the influx of this important second messenger and, therefore, there are many opportunities to study the quantitative control of Ca^{2+} influx in intact functioning tissues. Third, the ability of MEMRI to trace neuronal connections is opening up numerous possibilities for non-invasively imaging of neural networks. This should enable changes in the brain of an individual animal to be studied before and after a broad range of perturbations such as learning, plasticity, injury and repair. The combination of the ability to control the accumulation of Mn^{2+} in one region of the brain based on activity and then image the connections from that area should open novel strategies to study functional connectivity in the brain with MEMRI.⁸

A major challenge for the development of MEMRI is to increase sensitivity so that lower doses of Mn^{2+} can be used. Presently the doses used in animals are higher than what can be used in humans. Yet, subtle features of the neuroarchitecture, such as cortical layers, need even higher doses to cause a large enough gain in contrast. It would be very important to develop new ways to administer $MnCl_2$ directly to the target organ of interest without having to go to other vital organs, such as the heart, the liver and the kidneys during a systemic administration. Work towards accomplishing this goal has already begun. A couple of reports on direct, interechal administration of $MnCl_2$ shows good promise in delivering large amounts of $MnCl_2$ to the brain without the complications of a large systemic dose.^{22,49} The combination of clever ways to deliver Mn^{2+} with further improvements in the ability to detect Mn^{2+} would make it possible to use MEMRI in humans.

Acknowledgments

Special thanks go to Kathryn Sharer, Torri Wilson, Mary Angstadt, Daryl Despres and Keum Ho Lim for

excellent technical assistance. The authors also want to acknowledge Dr Hellmut Merkle for superb RF support. Support for the work comes from the Intramural Research Program, NINDS, directed by Eugene Major and Henry McFarland.

REFERENCES

- Lin YJ, Koretsky AP. Manganese ion enhances T_1 -weighted MRI during brain activation: an approach to direct imaging of brain function. *Magn. Reson. Med.* 1997; **38**: 378–388.
- Lin YJ. MRI of the rat and mouse brain after systemic administration of $MnCl_2$. Ph.D. Dissertation, Carnegie Mellon University, Pittsburgh, PA, 1997; 1–149.
- Duong TQ, Silva AC, Lee SP, Kim SG. Functional MRI of calcium-dependent synaptic activity: cross correlation with CBF and BOLD measurements. *Magn. Reson. Med.* 2000; **43**: 383–392.
- Aoki I, Tanaka C, Takegami T, Ebisu T, Umeda M, Fukunaga M, Fukuda K, Silva AC, Koretsky AP, Naruse S. Dynamic activity-induced manganese-dependent contrast magnetic resonance imaging (DAIM MRI). *Magn. Reson. Med.* 2002; **48**: 927–933.
- Hu TC, Pautler RG, MacGowan GA, Koretsky AP. Manganese-enhanced MRI of mouse heart during changes in inotropy. *Magn. Reson. Med.* 2001; **46**: 884–890.
- Krombach GA, Saeed M, Higgins CB, Novikov V, Wendland MF. Contrast-enhanced MR delineation of stunned myocardium with administration of $MnCl_2$ in rats. *Radiology* 2004; **230**: 183–190.
- Pautler RG, Silva AC, Koretsky AP. *In vivo* neuronal tract tracing using manganese-enhanced magnetic resonance imaging. *Magn. Reson. Med.* 1998; **40**: 740–748.
- Pautler RG, Koretsky AP. Tracing odor-induced activation in the olfactory bulbs of mice using manganese-enhanced magnetic resonance imaging. *Neuroimage* 2002; **16**: 441–448.
- Watanabe T, Michaelis T, Frahm J. Mapping of retinal projections in the living rat using high-resolution 3D gradient-echo MRI with Mn^{2+} -induced contrast. *Magn. Reson. Med.* 2001; **46**: 424–429.
- Lin CP, Tseng WY, Cheng HC, Chen JH. Validation of diffusion tensor magnetic resonance axonal fiber imaging with registered manganese-enhanced optic tracts. *Neuroimage* 2001; **14**: 1035–1047.
- Ryu S, Brown SL, Kolozsvary A, Ewing JR, Kim JH. Noninvasive detection of radiation-induced optic neuropathy by manganese-enhanced MRI. *Radiat. Res.* 2002; **157**: 500–505.
- Allegrini PR, Wiessner C. Three-dimensional MRI of cerebral projections in rat brain *in vivo* after intracortical injection of $MnCl_2$. *NMR Biomed.* 2003; **16**: 252–256.
- Van der LA, Verhoye M, Van MV, Tindemans I, Eens M, Absil P, Balthazart J. *In vivo* manganese-enhanced magnetic resonance imaging reveals connections and functional properties of the songbird vocal control system. *Neuroscience* 2002; **112**: 467–474.
- Saleem KS, Pauls JM, Augath M, Trinath T, Prause BA, Hashikawa T, Logothetis NK. Magnetic resonance imaging of neuronal connections in the macaque monkey. *Neuron* 2002; **34**: 685–700.
- Aoki I, Wu YJ, Silva AC, Lynch RM, Koretsky AP. *In vivo* detection of neuroarchitecture in the rodent brain using manganese-enhanced MRI. *Neuroimage* 2004; **22**: 1046–1059.
- Natt O, Watanabe T, Boretius S, Radulovic J, Frahm J, Michaelis T. High-resolution 3D MRI of mouse brain reveals small cerebral structures *in vivo*. *J. Neurosci. Meth.* 2002; **120**: 203–209.
- Watanabe T, Natt O, Boretius S, Frahm J, Michaelis T. *In vivo* 3D MRI staining of mouse brain after subcutaneous application of $MnCl_2$. *Magn. Reson. Med.* 2002; **48**: 852–859.
- Olanow CW. Manganese-induced parkinsonism and Parkinson's disease. *Ann. NY Acad. Sci.* 2004; **1012**: 209–223.
- Chandra SV, Shukla GS. Role of iron deficiency in inducing susceptibility to manganese toxicity. *Arch. Toxicol.* 1976; **35**: 319–323.
- Wolf GL, Baum L. Cardiovascular toxicity and tissue proton T_1 response to manganese injection in the dog and rabbit. *AJR Am. J. Roentgenol.* 1983; **141**: 193–197.
- Guyton AC. *Textbook of Medical Physiology*, Wonsiewicz MJ (ed.). WB Saunders: Philadelphia, PA, 1991; 1–1014.
- Morita H, Ogino T, Fujiki N, Tanaka K, Gotoh TM, Seo Y, Takamata A, Nakamura S, Murakami M. Sequence of forebrain activation induced by intraventricular injection of hypertonic NaCl detected by Mn^{2+} contrasted T_1 -weighted MRI. *Auton. Neurosci.* 2004; **113**: 43–54.
- Desoize B. Metals and metal compounds in carcinogenesis. *In Vivo* 2003; **17**: 529–539.
- Lee JH, Silva AC, Merkle H, Koretsky AP. Manganese-enhanced MRI (MEMRI) of mouse brain after systemic administration of $MnCl_2$: dose dependent and temporal evolution of T_1 contrast. *Magn. Reson. Med.* 2004 (in press).
- Mendonca-Dias MH, Gaggelli E, Lauterbur PC. Paramagnetic contrast agents in nuclear magnetic resonance medical imaging. *Semin. Nucl. Med.* 1983; **13**: 364–376.
- Fornasiero D, Bellen JC, Baker RJ, Chatterton BE. Paramagnetic complexes of manganese(II), iron(III), and gadolinium(III) as contrast agents for magnetic resonance imaging. The influence of stability constants on the biodistribution of radioactive aminopolycarboxylate complexes. *Invest. Radiol.* 1987; **22**: 322–327.
- Kang YS, Gore JC. Studies of tissue NMR relaxation enhancement by manganese: dose and time dependences. *Invest. Radiol.* 1984; **19**: 399–407.
- Nordhoy W, Anthonsen HW, Bruvold M, Jynge P, Krane J, Brurok H. Manganese ions as intracellular contrast agents: proton relaxation and calcium interactions in rat myocardium. *NMR Biomed.* 2003; **16**: 82–95.
- Nordhoy W, Anthonsen HW, Bruvold M, Brurok H, Skarra S, Krane J, Jynge P. Intracellular manganese ions provide strong T_1 relaxation in rat myocardium. *Magn. Reson. Med.* 2004; **52**: 506–514.
- Unger E, Fritz T, Shen DK, Wu G. Manganese-based liposomes. Comparative approaches. *Invest. Radiol.* 1993; **28**: 933–938.
- Mauss Y, Grucker D, Fornasiero D, Chambon J. NMR compartmentalization of free water in the perfused rat heart. *Magn. Reson. Med.* 1985; **2**: 187–194.
- Lauterbur PC, Mendonca-Dias M, Rudin A. Augmentation of tissue water proton spin-lattice relaxation rates by *in vivo* addition of paramagnetic ions. In *Frontiers of Biological Energetics*, Dutton P, Leigh JS, Scarpa A (eds). Academic Press: New York, 1978; 752–759.
- Hollis DP, Bulkley BH, Nunnally RL, Jacobus WE, Weisfeldt ML. Effect of manganese ion on phosphorus nuclear magnetic-resonance spectra of perfused rabbit heart—possible new membrane probe. *Clin. Res.* 1978; **26**: A240.
- Saeed M, Higgins CB, Geschwind JF, Wendland MF. T_1 -relaxation kinetics of extracellular, intracellular and intravascular MR contrast agents in normal and acutely reperfused infarcted myocardium using echo-planar MR imaging. *Eur. Radiol.* 2000; **10**: 310–318.
- Federle MP, Chezmar JL, Rubin DL, Weinreb JC, Freeny PC, Semelka RC, Brown JJ, Borello JA, Lee JK, Mattrey R, Dachman AH, Saini S, Harmon B, Fenstermacher M, Pelsang RE, Harms SE, Mitchell DG, Halford HH, Anderson MW, Johnson CD, Francis IR, Bova JG, Kenney PJ, Klippenstein DL, Foster GS, Turner DA. Safety and efficacy of mangafodipir trisodium (MnDPDP) injection for hepatic MRI in adults: results of the U.S. multicenter phase III clinical trials (safety). *J. Magn. Reson. Imag.* 2000; **12**: 186–197.
- Wendland MF, Saeed M, Lund G, Higgins CB. Contrast-enhanced MRI for quantification of myocardial viability. *J. Magn. Reson. Imag.* 1999; **10**: 694–702.
- Brurok H, Skoglund T, Berg K, Skarra S, Karlsson JO, Jynge P. Myocardial manganese elevation and proton relaxivity enhancement with manganese dipyrrodoxyl diphosphate. *Ex vivo* assessments in normally perfused and ischemic guinea pig hearts. *NMR Biomed.* 1999; **12**: 364–372.
- Bremerich J, Saeed M, Arheden H, Higgins CB, Wendland MF. Normal and infarcted myocardium: differentiation with cellular uptake of manganese at MR imaging in a rat model. *Radiology* 2000; **216**: 524–530.
- Gallez B, Bacic GG, Swartz HM. Evidence for the dissociation of the hepatobiliary MRI contrast agent Mn-DPDP. *Magn. Reson. Med.* 1996; **35**: 14–19.

40. Barbeau A. Manganese and extrapyramidal disorders (a critical review and tribute to Dr. George C. Cotzias). *Neurotoxicology* 1984; **5**: 13–35.
41. London RE, Toney G, Gabel SA, Funk A. Magnetic resonance imaging studies of the brains of anesthetized rats treated with manganese chloride. *Brain Res. Bull.* 1989; **23**: 229–235.
42. Wan XM, Fu TC, Smith PH, Brainard JR, London RE. Magnetic resonance imaging study of the rat cerebral ventricular system utilizing intracerebrally administered contrast agents. *Magn. Reson. Med.* 1991; **21**: 97–106.
43. Newland MC, Ceckler TL, Kordower JH, Weiss B. Visualizing manganese in the primate basal ganglia with magnetic resonance imaging. *Exp. Neurol.* 1989; **106**: 251–258.
44. Lucchini R, Albini E, Placidi D, Gasparotti R, Pigozzi MG, Montani G, Alessio L. Brain magnetic resonance imaging and manganese exposure. *Neurotoxicology* 2000; **21**: 769–775.
45. Murphy VA, Rosenberg JM, Smith QR, Rapoport SI. Elevation of brain manganese in calcium-deficient rats. *Neurotoxicology* 1991; **12**: 255–263.
46. Rabin O, Hegedus L, Bourre JM, Smith QR. Rapid brain uptake of manganese(II) across the blood-brain barrier. *J. Neurochem.* 1993; **61**: 509–517.
47. Sloat WN, Gramsbergen JB. Axonal transport of manganese and its relevance to selective neurotoxicity in the rat basal ganglia. *Brain Res.* 1994; **657**: 124–132.
48. Takeda A, Sawashita J, Okada S. Localization in rat brain of the trace metals, zinc and manganese, after intracerebroventricular injection. *Brain Res.* 1994; **658**: 252–254.
49. Liu CH, D'Arceuil HE, de Crespigny AJ. Direct CSF injection of MnCl₂ for dynamic manganese-enhanced MRI. *Magn. Reson. Med.* 2004; **51**: 978–987.
50. Drapeau P, Nachshen DA. Manganese fluxes and manganese-dependent neurotransmitter release in presynaptic nerve endings isolated from rat brain. *J. Physiol* 1984; **348**: 493–510.
51. Narita K, Kawasaki F, Kita H. Mn and Mg influxes through Ca channels of motor nerve terminals are prevented by verapamil in frogs. *Brain Res.* 1990; **510**: 289–295.
52. Hunter DR, Haworth RA, Berkoff HA. Cellular manganese uptake by the isolated perfused rat heart: a probe for the sarcolemma calcium channel. *J. Mol. Cell Cardiol.* 1981; **13**: 823–832.
53. Hallam TJ, Rink TJ. Agonists stimulate divalent cation channels in the plasma membrane of human platelets. *FEBS Lett.* 1985; **186**: 175–179.
54. Shibuya I, Douglas WW. Indications from Mn-quenching of Fura-2 fluorescence in melanotrophs that dopamine and baclofen close Ca channels that are spontaneously open but not those opened by high [K⁺]_o; and that Cd preferentially blocks the latter. *Cell Calcium* 1993; **14**: 33–44.
55. Neuwelt EA, Frenkel EP, Diehl JT, Maravilla KR, Vu LH, Clark WK, Rapoport SI, Barnett PA, Hill SA, Lewis SE, Ehle AL, Beyer CW Jr, Moore RJ. Osmotic blood-brain barrier disruption: a new means of increasing chemotherapeutic agent delivery. *Trans. Am. Neurol. Assoc.* 1979; **104**: 256–260.
56. Silva AC, Zhang W, Williams DS, Koretsky AP. Estimation of water extraction fractions in rat brain using magnetic resonance measurement of perfusion with arterial spin labeling. *Magn. Reson. Med.* 1997; **37**: 58–68.
57. Morita H, Ogino T, Seo Y, Fujiki N, Tanaka K, Takamata A, Nakamura S, Murakami M. Detection of hypothalamic activation by manganese ion contrasted T(1)-weighted magnetic resonance imaging in rats. *Neurosci. Lett.* 2002; **326**: 101–104.
58. Aoki I, Ebisu T, Tanaka C, Katsuta K, Fujikawa A, Umeda M, Fukunaga M, Takegami T, Shapiro EM, Naruse S. Detection of the anoxic depolarization of focal ischemia using manganese-enhanced MRI. *Magn. Reson. Med.* 2003; **50**: 7–12.
59. Vander EL, Colet JM, Muller RN. Spectroscopic and metabolic effects of MnCl₂ and MnDPDP on the isolated and perfused rat heart. *Invest. Radiol.* 1997; **32**: 581–588.
60. Tjalve H, Henriksson J, Tallkvist J, Larsson BS, Lindquist NG. Uptake of manganese and cadmium from the nasal mucosa into the central nervous system via olfactory pathways in rats. *Pharmac. Toxicol.* 1996; **79**: 347–356.
61. Pautler RG, Mongeau R, Jacobs RE. *In vivo* trans-synaptic tract tracing from the murine striatum and amygdala utilizing manganese enhanced MRI (MEMRI). *Magn. Reson. Med.* 2003; **50**: 33–39.
62. Tindemans I, Verhoye M, Balthazart J, Van der LA. *In vivo* dynamic ME-MRI reveals differential functional responses of RA- and area X-projecting neurons in the HVC of canaries exposed to conspecific song. *Eur. J. Neurosci.* 2003; **18**: 3352–3360.
63. Van Meir V, Verhoye M, Absil P, Eens M, Balthazart J, Van der Linden A. Differential effects of testosterone on neuronal populations and their connections in a sensorimotor brain nucleus controlling song production in songbirds: a manganese enhanced-magnetic resonance imaging study. *Neuroimage* 2004; **21**: 914–923.